Available online at www.sciencedirect.com
ScienceDirect
Trans. Nonferrous Met. Soc. China 33(2023) 2955−2969
Transactions of Nonferrous Metals Society of China
www.tnmsc.cn

Improved mechanical properties of Mg−3Al−1Zn alloy sheets with TD-preferred texture prepared via turned bearing extrusion

Lin-tao LIU[1], Sheng-wen BAI[1], Bin JIANG[1,2], Chao HE[1], Qing-hang WANG[3], Ming YUAN[1], Guang-sheng HUANG[1], Ding-fei ZHANG[1], Fu-sheng PAN[1,2]

1. National Engineering Research Center for Magnesium Alloys, Chongqing University, Chongqing 400044, China;
2. Chongqing Academy of Science and Technology, Chongqing 401123, China;
3. School of Mechanical Engineering, Yangzhou University, Yangzhou 225127, China

Received 24 March 2022; accepted 15 June 2022

Abstract: To improve the ductility and formability of the Mg−3Al−1Zn alloy sheets, novel turned bearing extrusion (TBE) dies are designed based on the conventional extrusion (CE) die. Finite element simulations are performed to catch the distributions of strains and temperature fields during extrusion. The results show that gradient distribution of strain along the normal direction (ND) in TBE dies leads to the gradient microstructure. Furthermore, the transversal direction (TD)-preferred texture with ND-oriented grains deflecting toward extrusion direction (ED) is achieved. The TD-preferred texture is generated by the more activated non-basal slips in the TBE due to the higher temperature at a higher strain than that in the CE die. Because of the texture modification, the ductility and bendability of the TBE sheets. The elongation of the TBE-6 sheet reaches 33% and the bending angle reaches 83.5° when the sample is tested along 45° direction.

Key words: turned bearing extrusion; TD-preferred texture; plasticity; bendability; gradient grain size

1 Introduction

As the lightest structural metallic materials, Mg and its alloys are promising materials because of their high specific stiffness and specific strength [1−3]. At present, Mg alloys for industrial applications are mostly casting products. However, the defects in the products caused by the casting process such as shrinkage and porosity limit the application of casting components which can be avoided in the wrought Mg alloys [3,4]. Disappointedly, the strong basal texture of wrought Mg alloys originating from manufacture processes results in the poor plasticity and formability [5]. In recent years, a lot of efforts have been made to improve the plasticity and formability of the Mg alloy sheets [6−9].

As the most universal processing method to optimize the microstructure and texture of wrought Mg alloys, severe plastic deformation (SPD), such as equal channel angular pressing (ECAP) [10,11], cyclic extrusion compression (CEC) [12] and accumulative alternating back extrusion (AABE) [8], is usually used to improve the mechanical properties. KIM et al [10] found that the grain size of the AZ61 Mg alloy prepared by ECAP was gradually reduced with increasing the processing passes. It was explained that the plasticity of the alloy increased after ECAP due to the activation of more slip systems during tensile tests caused by grain refinement. WANG et al [8] prepared the AZ31 through AABE method. As the processing passes of AABE increased to 4, the grains of the

Corresponding author: Sheng-wen BAI, Tel: +86-18810305537, E-mail: baisw@cqu.edu.cn;
Bin JIANG, Tel: +86-13594190166, E-mail: jiangbinrong@cqu.edu.cn
DOI: 10.1016/S1003-6326(23)66310-1

alloy were significantly refined and the texture was weakened. As a result, the elongation along extrusion direction (ED), 41° direction (the deflection angle direction from ED to transverse direction) and transverse direction (TD) increased by about 8%, 7%, and 11%, respectively. The texture modification was attributed to the increase of ⟨*c*+*a*⟩ slip.

SPD has remarkable effects on texture weakening and grain refinement. However, SPD is often used to prepare materials in small-scale [3,13]. The commercial extrusion is more advantageous than the SPD methods in the fabrication of Mg alloy products for industrial application. To combine texture weakening with production efficiency, asymmetrical extrusion was developed. As numerically simulated by CHEN et al [14], in the conventional extrusion, the strain along normal direction (ND) was symmetrical, which was responsible for the basal texture. But the strain distribution during extrusion in the asymmetric processing methods was changed [15], which was simulated in the research of XU et al [16]. Based on this theory, YANG et al [17] designed asymmetric extrusion dies with unequal bearings. The lengths of the upper and lower surfaces of die bearings were unequal, resulting in additional shear strain during the extrusion. The texture was deflected by about 20° toward ED which led to the elongation along ED, 45° (the half angle between ED and TD) and TD increased by 1%, 2% and 4%, respectively. The additional asymmetric shear strain was the main reason for texture deflection. WANG et al [18] extruded AZ31 Mg alloy sheets by using the asymmetric porthole extrusion (APE) dies with different bridge angles. The texture was more weakened with increasing the bridge angle of the die. Compared with the sheets extruded by the conventional die, the Erickson cupping index value of APE-90 sheets exceeded that of conventional extrusion sheets by 74% because of texture weakening. These researches indicate that the asymmetric processing technology is effective in microstructure refinement and texture weakening and therefore can improve the plasticity and formability of Mg alloy sheets. However, the texture in these studies are deflected toward single direction, namely ED, which is mediocre to improve the plasticity and formability.

In this study, a novel asymmetric die design, termed the turned bearing extrusion (TBE) die, was developed, in which the shear zone was designed to add the extra shear strain to conventional extruded stain. Mg−3Al−1Zn alloy sheets with TD-preferred texture and grain size gradient were produced via the TBE at 450 °C. The microstructures, tensile properties and bendability of TBE sheets were evaluated. Finite element simulations were carried out to calculate the state variables during the extrusion. This work fills the gaps of TD-preferred texture and gradient microstructure in AZ31 alloy sheets prepared by single pass extrusion, which provides another significant method to fabricate AZ31 alloy sheets with high plasticity and bendability.

2 Experimental

To enhance the shear strain, two turned bearing extrusion dies were specially designed. Figure 1 shows the schematic diagram of the dies and bearings. Turned corners with heights of 1.5 mm (Figs. 1(g, h)) were introduced in the two turned bearing extrusion dies, denoted as TBE-3 and TBE-6. The turned corners had shear zones with widths of 3 and 6 mm for TBE-3 and TBE-6, respectively (Figs. 1(g, h)). The conventional extrusion (CE) die was employed as the case for comparison (Fig. 1(c)). The dimensions of the die orifices were all 56 mm × 3 mm, and the extrusion ratios were 29.9:1.

The commercial AZ31 Mg alloy billets (Mg−3.05Al−1.01Zn−0.55Mn, wt.%) was employed in this study. The billets were cut into cylinders with the dimensions of *d*80 mm × 120 mm. To remove the dendrites, homogenization was conducted in resistance furnace at 450 °C for 12 h, followed by water cooling. Before extrusion, the billets were preheated to 450 °C and soaked at this temperature for 2 h. Thereafter, the extrusion experiments were carried out by an extruder with the ram speed of 1.1 mm/s. The Mg alloy sheets were cooled in air when it was extruded out from the die orifice. The cross-sectional dimensions of the extruded sheets are 56 mm × 3 mm.

Bending experiments were carried out by a V-shaped die setup with an angle of 90° and chamfer radius of 4 mm (Fig. 2(a)). Bending samples had the dimensions of 50 mm × 12 mm × 3 mm in length, width and thickness, respectively.

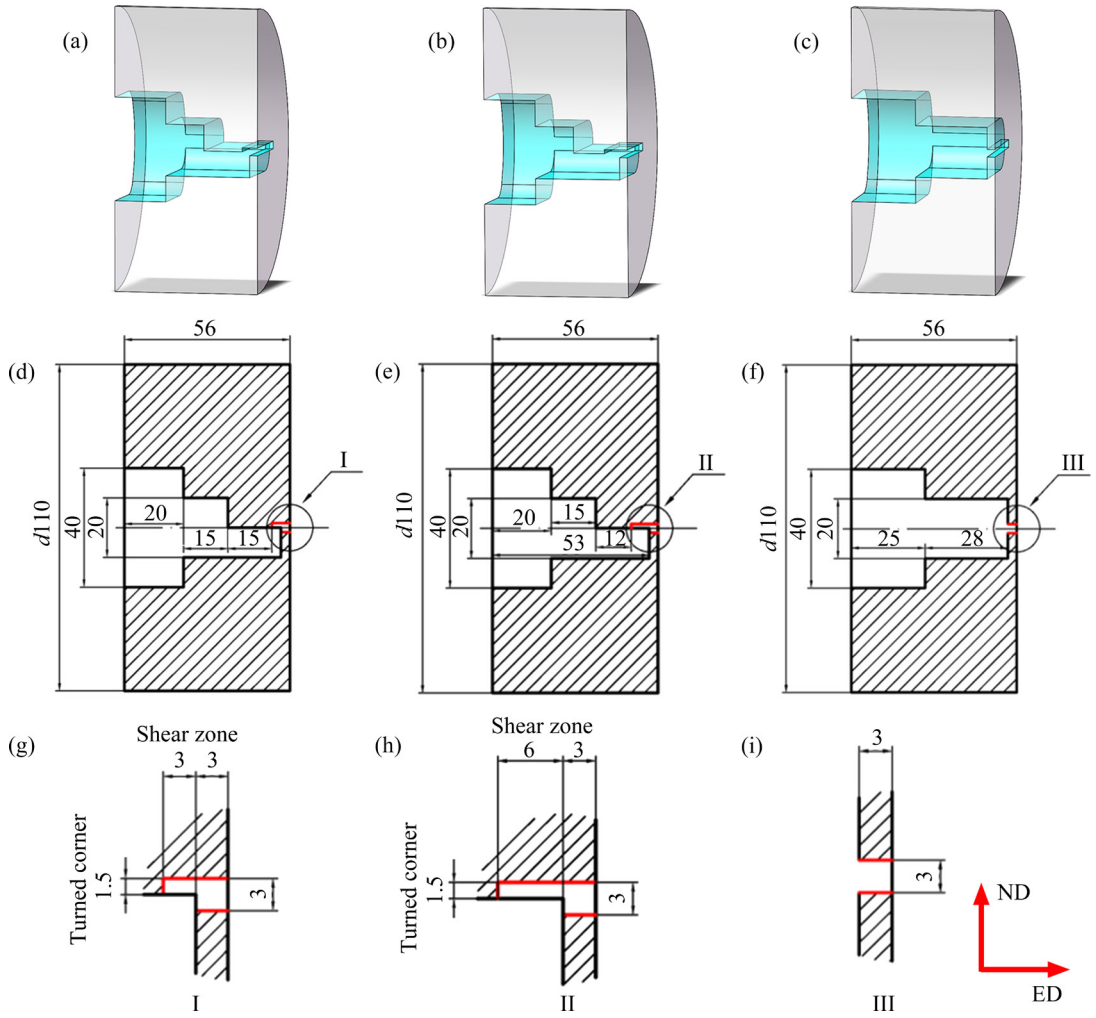

Fig. 1 Schematic diagrams and dimensions of TBE-3 (a, d, g), TBE-6 (b, e, h) and CE (c, f, i) dies (Unit: mm)

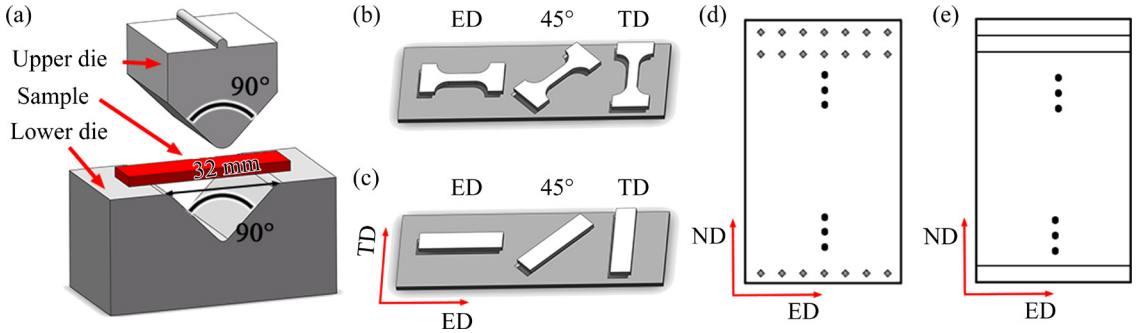

Fig. 2 Schematic diagrams of bending experiments (a), tensile specimens (b), bending specimens (c), positions of hardness measurement (d) and method for partitioning grain size (e)

To investigate the effects of gradient microstructure on bendability, each group of tests included two cases, namely placing the coarse-grained region (CG) and the fine-grained region (FG) of the sheets outside.

Tension and compression tests were conducted by a universal testing machine (CMT6305−300 kN) at ambient temperature to evaluate the mechanical properties of the extruded Mg alloy sheets. Dog-bone-shaped tensile specimens, with dimensions of 12 mm × 6 mm × 3 mm in gauge length, width and thickness, respectively, were cut along ED, 45° direction and TD of each sheet (Fig. 2(b)). Compression samples were cut into rectangles with dimensions of 9 mm × 6 mm × 3 mm in length, width and thickness, respectively. along ED, 45°

direction and TD. The strain rate was set to be 2.7×10^{-3} s^{-1}. The tests of the specimens under the same condition were repeated three times to ensure the reproducibility of the data.

Hardness on ED−ND planes of samples was measured by Vickers microhardness tester (HVS−1000Z) with a load of 20 N and a dwell time of 15 s. The measured planes were ground to mirror surface by the 1200# sandpaper. Several lines parallel to ED were marked on the ED−ND plane, and the hardness values of 7 points on each line were measured by the tester (Fig. 2(d)). The average hardness value of these 7 points on each line represented the hardness of the position where the line was located.

The optical microscope (OM, ZEISS Axiovert 40 MAT), electron backscattered diffraction (EBSD, JEOL JSM−7800F) and transmission electron microscopy (TEM, FEI Talos F200S) were employed to observe the microstructure. After grinding with 1200# SiC sandpaper, samples were etched by the saturated picric acid solution (1.5 g picric acid, 5 mL acetic acid, and 25 mL ethyl alcohol) and observed by OM. To register the heterogeneity of grain size, the micrographs of the ED−ND planes were divided into 16 grids parallel to ED (Fig. 2(e)). The grains in each grid were completely counted, which were used to calculate the grain size distribution along ND. For EBSD tests, samples were ground with 1200# sandpaper, and electropolished by the AC2 electrolytic solution for 90 s. The polishing temperature was −25 °C and the voltage was set to be 20 V. The samples for TEM were ground to 50 μm and then prepared with ion beam thinning (GATAN, PIPS 691). The accelerating voltage for TEM observation was 200 kV.

Finite element simulations were carried out by the commercial software DEFORM-3D to calculate the distributions of temperatures and strains in the cavities of dies. The process parameters of finite element simulations, i.e., billet temperature (450 °C) and ram speed (1.1 mm/s), were as same as those of extrusion experiments. The extrusion simulations were based on the constitutive models of AZ31 alloy researched in Refs. [19,20]. Heat exchanges between the billet, extrusion tooling, and surrounding environment were allowed during the simulations. The thermal conductivity coefficient between billet and tooling was set to be 11 N/(°C·s·mm^2). A shear friction model was adopted at the interfaces between the billet and extrusion tooling and the friction coefficient was set to be 1 [21].

3 Results

3.1 Microstructure

Figure 3 shows the microstructure of the as-homogenized AZ31 alloy. The average grain size is 144.7 μm. No dendrite is found under the OM and scanning electron microscope. In the scanning electron microscope micrograph, some strip-shaped particles exist. The particles are Al−Mn phases which are difficult to dissolve in α-Mg matrix [22]. Figure 4 shows the OM images of the as-extruded sheets produced by TBE-3, TBE-6 and CE. All grains along ND, namely the whole thickness, are observed. The nearly complete dynamic recrystallization (DRX) is observed in the OM micrographs. In addition, a little elongated filamentous grain is observed. The distributions of grain size in TBE-3 and TBE-6 samples exhibit gradient structures along ND. The grain size in the fine-grained side (FG) of TBE-3 sample is 11.6 μm, and it gradually increases to 74.8 μm in the middle layer, and finally drops to 51.1 μm (Figs. 4(a, d)).

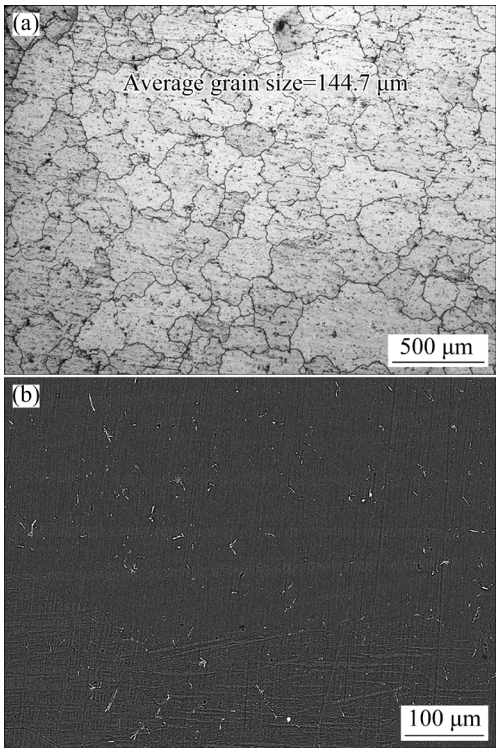

Fig. 3 OM (a) and scanning electron microscope (b) micrographs of as-homogenized AZ31 billets

The grain size of FG side in TBE-6 sheet is 12.4 μm, and it rapidly increases to 81.1 μm, and eventually decreases to 45.6 μm along ND (Figs. 4(b, d)). CE sample shows uniform and fine grains (Fig. 4(c)). The grain size of CE sheet is varied from 12.5 μm near the surface to 14.7 μm in the middle (Fig. 4(d)). The curves show the grain sizes of FG side of TBE-3 and TBE-6 sheets are similar, but the grain size of coarse grain region in TBE-6 is larger than that in TBE-3. The coarsest grains in TBE-3 and TBE-6 are almost as large as the as-homogenized grains, which can be the evidence of abnormal grain growth. The distribution of microhardness along ND is presented in Fig. 4(e). Hardness values of the Mg alloy sheets are in good agreement with the grain sizes.

3.2 Texture of as-extruded AZ31 sheets

Figure 5 shows inverse pole figure (IPF) maps and pole figures of TBE-3, TBE-6, and CE samples. TBE-3 and TBE-6 samples present TD-preferred texture in which the most *c*-axis of grains are parallel to TD with the residual ND-oriented grains titling towards ED. The maximum relative density of TBE-6 sheets is slightly higher than that of TBE-3 sheets. Such a texture type is unusual in the traditional as-extruded AZ31 alloys. The most common texture in wrought AZ31 alloy is strong basal texture with the *c*-axis of most grains parallel to ND [8,23,24]. In TBE-3 and TBE-6 sheets, the basal texture oriented grains have deflected orientations toward ED. The deflection angles of TBE-3 sheets and TBE-6 sheets are 15° and 12°, respectively. Such deflection is similar with the previous studies [15,17,25].

3.3 Mechanical properties and bending performance

Figure 6 depicts tension and compression true strain−stress curves of TBE-3, TBE-6, and CE sheets along ED, 45° direction, and TD, respectively. Mechanical properties of as-extruded sheets are listed in Table 1. When tested along ED, the tensile yield strengths (TYSs) of TBE-3 sheets (151.8 MPa) and TBE-6 sheets (176.1 MPa) are 30.5 and 6.2 MPa lower than the TYS of CE sheets (182.3 MPa), respectively. The tensile elongations (TEL) of TBE-3 and TBE-6 sheets are 1.8% and 1.6% higher than the elongation of CE sheets. The tension curves along 45° direction show that TBE-3

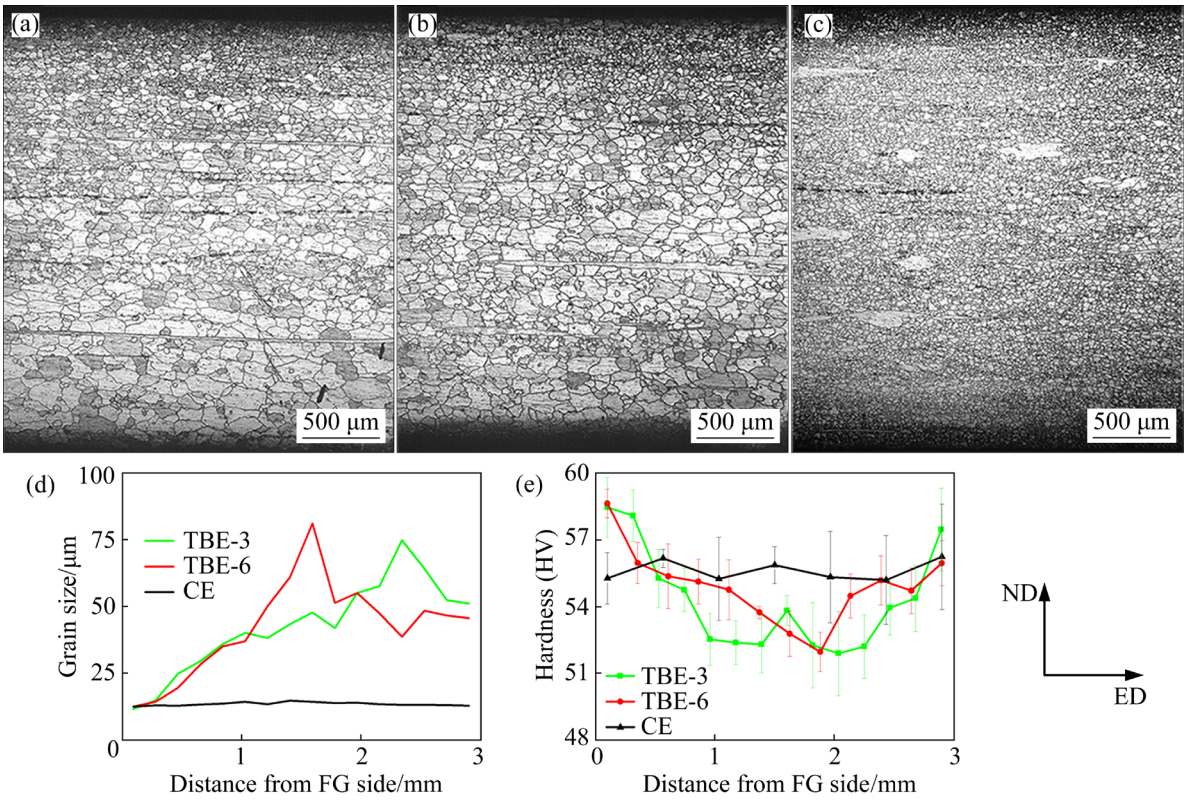

Fig. 4 Micrographs of Mg alloy sheets produced by TBE-3 (a), TBE-6 (b) and CE (c), and distribution curves of grain size (d) and microhardness (e)

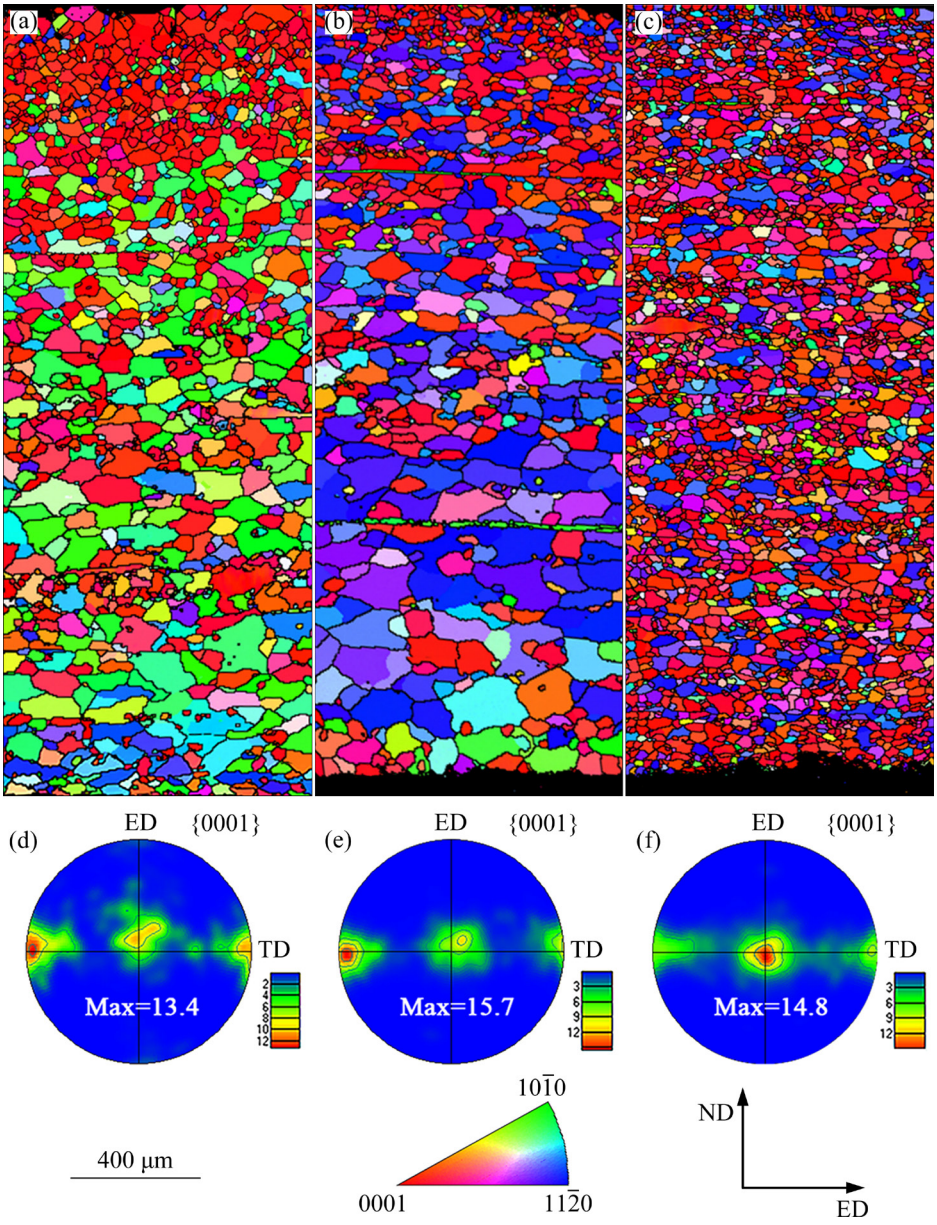

Fig. 5 IPF maps (a, b, c) and pole figures (d, e, f) of TBE-3 (a, d), TBE-6 (b, e), and CE (c, f) samples on ED−ND planes

sheets and TBE-6 sheets possess preeminent TELs of 33.0% and 31.4% which are 11.6% and 10% higher than the elongation of CE sheets (21.4%). When tested along TD, the TYSs of TBE-3 sheets (64.2 MPa) and TBE-6 sheets (68.7 MPa) are 50.2 and 45.7 MPa lower than the TYS of CE sheets (114.4 MPa), respectively. The compression curves of CE sheets exhibit S-shape along all tested directions. However, the compression curves of TBE-3 and TBE-6 sheets along 45° direction and TD are not S-shaped. The compressive yield strengths (CYS) of CE sheets along ED, 45° direction and TD are 92.4, 81.3 and 90.0 MPa, respectively. TBE-6 sheets present lower CYSs along ED (65.2 MPa) and 45° direction (64.6 MPa) than TD (107.5 MPa). The TD-preferred texture dominates the deformation behavior of TBE-3 and TBE-6 sheets.

Figure 7 shows the bending performance of TBE-3, TBE-6 and CE sheets. The histograms express the bending angles of the samples which contain the springback due to unloading. When tested along ED (Fig. 7(a)), TBE-6 samples can be successfully bent until the samples fit the surfaces of die with 90° angle. Both TBE-3 and CE samples are cracked before the samples are formed. The

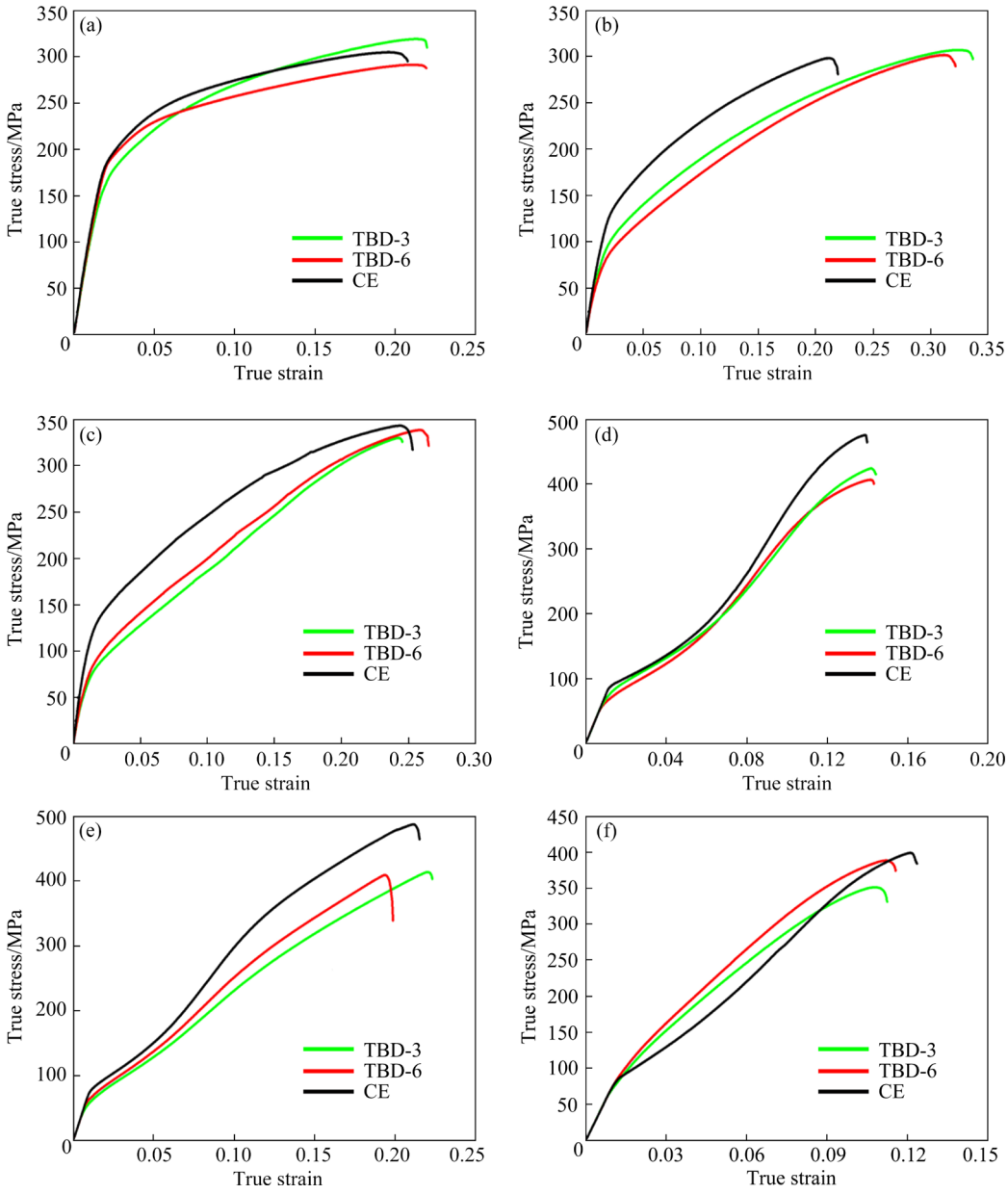

Fig. 6 Tension (a, b, c) and compression (d, e, f) true stress−strain curves of TBE-3, TBE-6, and CE sheets along ED (a, d), 45° direction (b, e), and TD (c, f)

Table 1 Mechanical properties along ED, 45° direction, and TD of TBE-3, TBE-6, and CE sheets

Sheet	Direction	TYS/ MPa	UTS/ MPa	TEL/ %	CYS/ MPa	CYS/ TYS
TBE-3	0°	151.8	320.0	21.9	75.6	0.498
	45°	88.2	308.2	33.0	55.3	0.627
	90°	64.2	331.0	24.3	92.3	1.438
TBE-6	0°	176.1	293.2	21.7	65.2	0.370
	45°	68.9	302.1	31.4	64.6	0.938
	90°	68.7	340.5	26.0	107.5	1.565
CE	0°	182.3	306.2	20.1	92.4	0.507
	45°	128.0	298.6	21.4	81.3	0.635
	90°	114.4	343.5	24.4	90.0	0.787

results indicate the TBE-6 sheets possess superior bendability to TBE-3 and CE sheets. As for bending properties along 45° direction, TBE-3 and TBE-6 sheets can be formed without macroscopic crack, while the CE samples are cracked during the bending experiments (Fig. 7(d)). The preeminent bending performance of TBE-3 and TBE-6 sheets is attributed to the TD-preferred texture dominantly. When tested along TD, all TBE-3, TBE-6 and CE samples fail to form. The distinction of bending performance along TD of the three kind of sheets is negligible. It can be concluded that the bendability of TBE-3 sheets and TBE-6 sheets is superior to CE

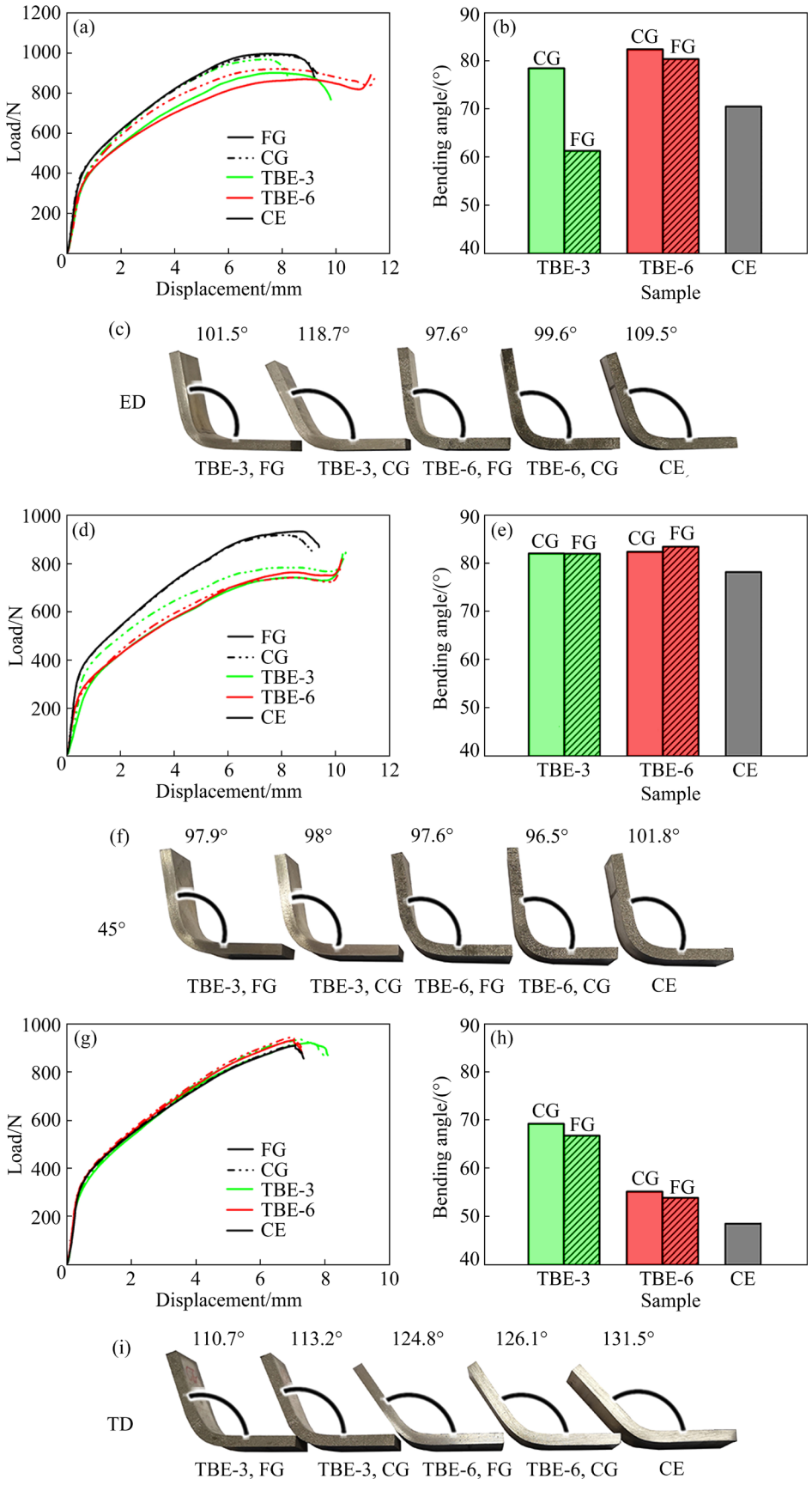

Fig. 7 Bending curves (a, d, g), bending angles (b, e, h) and tested samples (c, f, i) of TBE-3, TBE-6, and CE sheets along ED (a−c), 45° direction (d−f) and TD (g−i) (FG−Fine-grained region; CG−Coarse-grained region)

sheets, and TBE-6 sheets possess the best bendability which can be formed without a macroscopic crack along ED and 45° direction.

4 Discussion

4.1 Formation of gradient microstructure

It is well known that the grain size of wrought Mg alloy is deeply influenced by strain during the hot working. Extra shear strain [26], higher extrusion ratio [27] and higher rolling reduction [28] can increase strain during hot working. By these ways, grain size is refined by creating more strain energy for nucleation. In this study, strains near the bearing of TBE dies are designed to be gradient to prepare material with gradient microstructure.

The distributions of the equivalent strains during the steady extrusion state are analyzed to reveal the relationship between the strain field and the grain size distribution (Fig. 8). In all extrusion cases, the maximum strain is distributed in the region near the die bearing (Figs. 8(a−c)). This demonstrates that the DRX in above-mentioned position is the most intense. Therefore, the analysis of the equivalent strain is mainly focused on this position. The strain near the die orifice is traced along the arrow marked in Figs. 8(a−c). The strain−distance curves are plotted in Fig. 8(d) where the distance represents the length between the monitored point and lower surface of the sheet (surface of FG side in Fig. 4). The equivalent strains along the arrows in TBE-3 and TBE-6 exhibit a trend of decreasing first and then increasing. The equivalent strain along the arrows in CE shows stable trend less than 0.2. Such distribution of the strain is in good agreement with that of the grain size in OM images (Fig. 4). In TBE-3 and TBE-6 dies, the equivalent strains close to the surfaces are larger than those inside the cavities. More strain energy is generated at a larger strain, thereby promoting the nucleation of DRX and the formation of fine grains. Consequently, it can be inferred that the gradient in grain size of the TBE sheets is mainly caused by the gradient in strain distribution.

The strains near the die orifices of the TBE are higher than those of CE (Fig. 8(d)), but the average grain sizes of TBE sheets are larger compared with the CE sheets. Besides the strain, the temperature also plays an important role in the microstructure evolution of Mg alloy during the extrusion. Due to heat generated by friction and extrusion strain, larger strain and extrusion speed increase the extrusion temperature near the bearing [29−31]. As a result, the driving force of grain growth increases, and grain growth is more rapid. Therefore, in this work, coarser grains in the TBE sheets are formed due to the higher temperature compared with the CE sheets (Fig. 9).

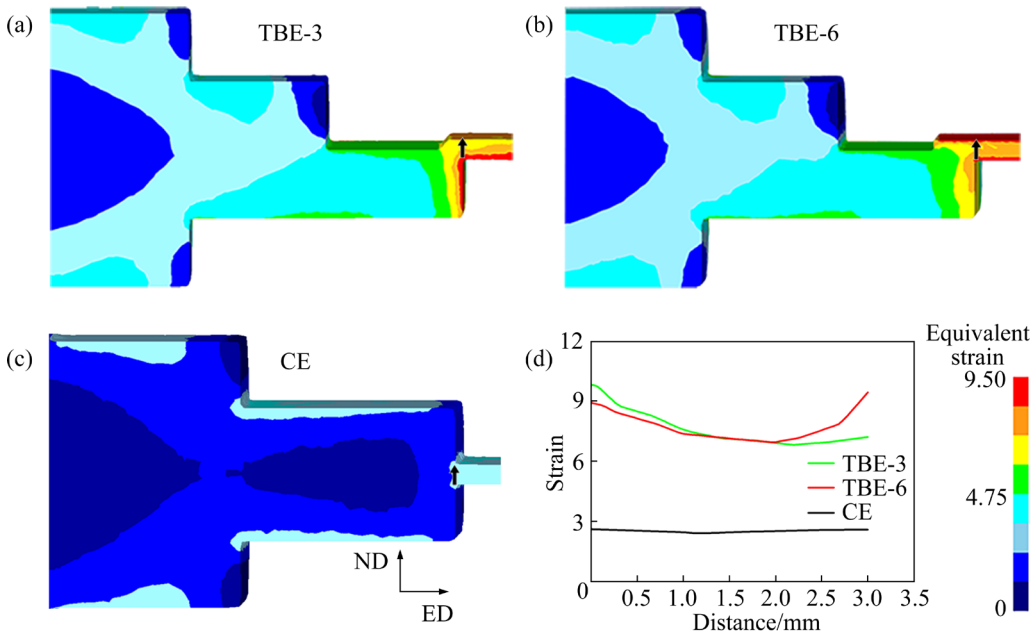

Fig. 8 Simulated equivalent strains in TBE-3 (a), TBE-6 (b), and CE (c) samples at steady extrusion state and distributions of strain along arrows (d)

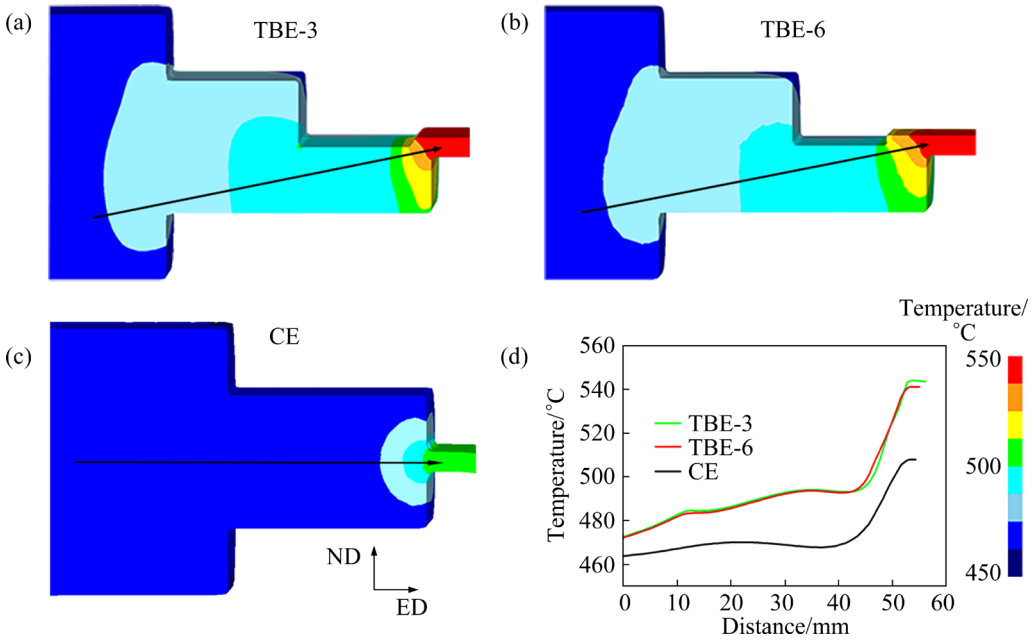

Fig. 9 Simulated temperatures of TBE-3 (a), TBE-6 (b), and CE (c) samples at steady extrusion state and distributions of temperature along arrows (d)

4.2 Formation of TD-preferred texture

The modification of texture in wrought Mg alloy with double-peak texture is mainly due to the activation of non-basal slip. The addition of rare earth elements leads to pyramidal ⟨*c*+*a*⟩ slip and results in texture deflection in the as-extruded Mg alloy sheet [32−34]. AGNEW et al [35] carried out numerical simulations on Mg−Y alloys during texture evolution. They found that the activation of pyramidal ⟨*c*+*a*⟩ slip in Mg−Y alloy deflected the texture toward the direction perpendicular to the compression axis. LYU et al [36] found that, in the Mg−Y−Sm−Zn−Zr alloy prepared with indirect extrusion at 420 °C, pyramidal-II slip rotated the orientation of grains toward the direction perpendicular to the compression axis, which caused TD deflected texture. It is proven that the activation of pyramidal ⟨*c*+*a*⟩ slip can bring about TD-preferred texture. High temperature can also activate the non-basal slip and deflect the texture of Mg alloy. According to the research [37], at a superhigh temperature, the values of critical resolved shear stress (CRSS) of prismatic ⟨*a*⟩ slip, pyramidal ⟨*c*+*a*⟩ slip in AZ31 were close. Massive non-basal slips took place during the deformation.

During extrusion process, the increase of temperature is the result of the heat generated by friction and plastic deformation [31]. Figure 9 presents the simulated temperatures in TBE-3, TBE-6, and CE. The temperature distributions are traced by arrows and are presented in Fig. 9(d). The increase of temperatures mainly occurs near the die orifices where the strains are the highest. Temperatures near the die orifice of TBE-3, TBE-6 and CE reach 544, 541 and 507 °C, respectively. The temperature in TBE-3 and TBE-6 is much higher than that in CE, because more heat is generated at a larger equivalent strain in the TBE dies. The superhigh temperature in TBE dies activates abundant non-basal slips.

Figure 10 shows the dislocations observed near the die orifice of TBE-6. To observe the non-basal dislocations during extrusion, the extrusion experiment was interrupted. The sampling method is shown in Fig. 10(a). The non-basal dislocations can be identified with the criterion, $\boldsymbol{g}\cdot\boldsymbol{b}=0$ ($\boldsymbol{b}$ is Burger vector) [38]. With $\boldsymbol{g}=0002$, basal ⟨*a*⟩ dislocation has no contrast, and only ⟨*c*⟩ and ⟨*c*+*a*⟩ dislocations can be observed. In other words, the dislocations in Fig. 10(c) are non-basal dislocations, including ⟨*c*⟩ and ⟨*c*+*a*⟩ dislocations. Compared with total dislocations (Fig. 10(b)), non-basal dislocations (Fig. 10(c)) accounts for a large proportion. In Fig. 10(c), nano-scaled cell substructure can be observed, which is coarsened by absorbing dislocations during later deformation.

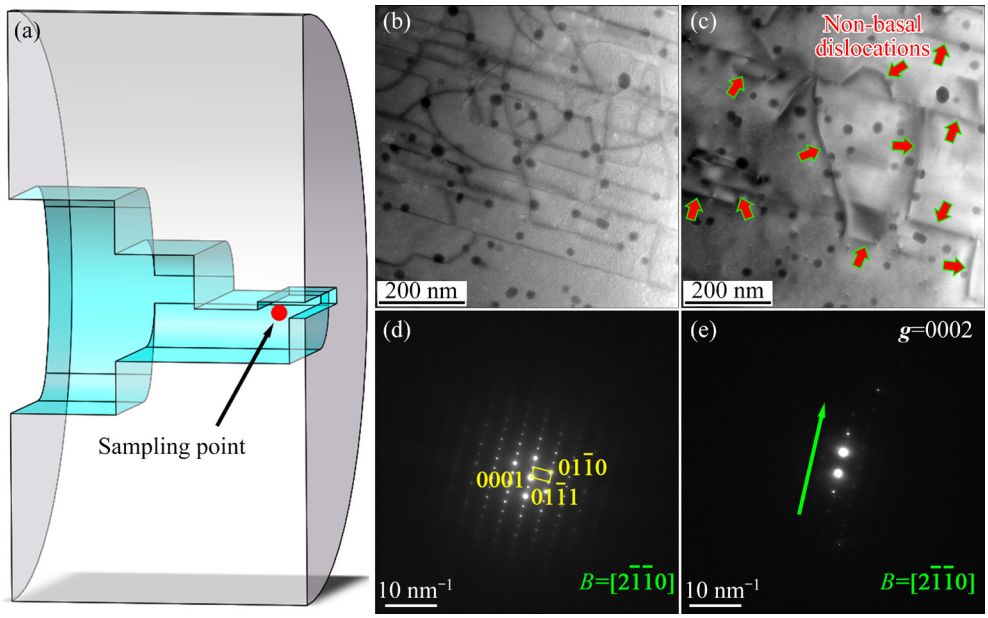

Fig. 10 Schematic diagram of TEM sampling method (a), HAADF bright field images of total dislocations and selected area electron diffraction patterns (b, d), and HAADF bright field images with diffraction condition of two beams and diffraction vector of $\boldsymbol{g}$=0002 (c, e)

Combined with the simulated temperature results and observed non-basal dislocations, it can be inferred that the TD-dominated texture is the result of the activation of abundant non-basal slips. With the activation of non-basal slips, the *c* axis of grains deflected along the compressed direction, and TD preferred texture came out [36]. To sum up, the formation of TD-preferred texture in this work is mainly attributed to the activation of non-basal slip caused by the superhigh temperature.

4.3 Effects of texture and gradient grain size on mechanical properties

The TYSs along ED, 45° direction and TD of TBE sheets are lower than the TYS of CE sheets. The grain size effect of TBE sheets plays a partial role in the decrease of TYSs. The proportion of grain size in the TBE sheets larger than that of CE sheets accounts for about 11/12 of the thickness (Fig. 4(d)). According to the Hall−Petch law, the coarser grains in the TBE sheets can weaken the blocking effect of grain boundary on dislocation slip and further reduce TYS [39−42]. Grain size effect also partially explains why the CYSs of TBE sheets along ED are lower than the CYS of CE sheets in which the predominant deformation mechanism is the $\{10\bar{1}2\}$ twinning. When compressed along ED, 45° direction and TD, the deformation mechanism of CE samples is mainly $\{10\bar{1}2\}$ twinning owing to its strong basal texture, which can be reflected in the S-shaped compression curves of CE samples in Fig. 6. When compression tests are carried out along ED, 45° direction and TD, due to TD-preferred texture, angles between axes of compression stresses and *c*-axes of most grains in TBE sheets are about 90°, 45°, and 0°, respectively. Consequently, the deformation modes of TBE samples are dominated by $\{10\bar{1}2\}$ twinning, basal $\langle a\rangle$ slip and prismatic slip, respectively. As a result, the CYSs of TBE sheets along ED and 45° direction are lower than the CYS of CE sheets, while it is a little higher than the CYS of CE sheets along TD.

Besides the effect of grain size, texture is another dominant factor in tensile tests. Basal texture with *c* axis parallel to ND is the hard orientation for AZ31 alloy sheet, whether the tensile stress is along ED, 45° direction or TD [43]. When tensile stress is imposed along the ED−TD plane of the sheet, basal slip and $\{10\bar{1}2\}$ twinning which have low CRSS at room temperature are difficult to activate. The SFs of grains with basal texture are low for basal slip and $\{10\bar{1}2\}$ twinning under such stress conditions [44,45]. Table 2 shows the average SFs for basal slip when tensile stress is imposed along ED, 45° direction and TD. The TD-preferred texture obtained by TBE is not the same as the basal texture. In this work, the texture

Table 2 Average SF of basal ⟨*a*⟩ slip in grains of TBE-3, TBE-6 and CE sheets

TBE-3			TBE-6			CE		
ED	45° direction	TD	ED	45° direction	TD	ED	45° direction	TD
0.159	0.373	0.203	0.117	0.417	0.096	0.092	0.279	0.228

obtained by TBE can be divided into two parts: the basal component and the TD-oriented component. The ND-oriented grains in TBE-3 and TBE-6 sheets deviate by 15° and 12° from ND, respectively, which gives higher SFs for basal slip (0.159 for TBE-3 and 0.117 for TBE-6). This explains the decrease of TYS and the increase of TEL along ED for TBE-3 and TBE-6 sheets.

TD-oriented grains possess soft orientation when tensile stress is imposed along 45° direction. TD-oriented grains have high SFs (0.373 for TBE-3 sheets and 0.417 for TBE-6 sheets) for basal slip. High SFs for basal slip are attributed to much higher TEL of TBE-3 (33.0%) and TBE-6 (31.4%) sheets compared with CE sheets (21.4%). The plasticity of TBE sheets along 45° direction is higher than that in some other related studies. For example, the TEL along 45° direction of the wrought AZ31 alloy sheets in some previous studies was 22.4% [46], 27.3% [47] and 24.5% [48]. When tensile tests are carried out along TD, the dominant deformation modes in CE is prismatic ⟨*a*⟩ slip because of the strong basal texture. But the TEL along TD is larger than that along ED. Higher SF for basal ⟨*a*⟩ slip is the key factor for the larger TEL. When stretched along TD, the dominant deformation mechanisms in the TBE sheets are $\{10\bar{1}2\}$ twinning in the early stage and prismatic ⟨*a*⟩ slip in the following stage. For the CRSS of prismatic ⟨*a*⟩ slip is larger than that of $\{10\bar{1}2\}$ twinning, the TYSs of TBE sheets are lower than those of CE sheets. Due to the coordinated deformation of multiple deformation mechanisms, TBE sheets exhibit similar TELs as CE sheet.

In the bending experiment of this study, failure occurs at the outer side of the sample. During the bending process, the tensile stress in the outer region and the compressive stress in the inner region were widely reported [49−51]. As discussed above, ED-deflected grains in TBE sheets endow these grains with higher SFs for the basal slip. Similarly, TBE samples along 45° direction possess high SFs, while it is relatively low for CE samples. As a result, the bendability of TBE sheets along ED and 45° direction is more preeminent than that of CE sheets.

The TD-preferred textures have dominant effects on plasticity and bendability. Besides, the existence of gradient microstructures is beneficial to the improvement of bendability. In the research by HE et al [52], the AZ31 alloy plates with coarser grain showed better bendability. It was explained that microcracks nucleation was shifted from nucleation along grain boundaries to nucleation at interior of grains. The generation of microcracks is delayed by coarse grains in the outer region. The stress state of inner regions of bending samples is compression along ED, which can lead to $\{10\bar{1}2\}$ twinning. The original texture is strong TD-preferred texture which is unfavorable for basal ⟨*a*⟩ slip. However, after complete twinning, the texture becomes stronger and is more unfavorable for basal ⟨*a*⟩ slip [44,53,54]. According to Ref. [41], the coarser the grains are, the easier the $\{10\bar{1}2\}$ twinning takes place. As a result, the inner region with coarser grain is more difficult to accommodate the strain after complete twinning. Therefore, The CG samples of TBE-3 show improved bendability than FG samples of TBE-3 and CE samples.

5 Conclusions

(1) Gradients in grain size are obtained in the sheets prepared by TBE at the billet temperature of 450 °C, due to the gradient of strain along ND.

(2) During TBE, higher strain increases extrusion temperature in the bearing zone compared with CE. Such a superhigh temperature results in the activation of non-basal slip, and further causes TD-preferred texture.

(3) For the basal ⟨*a*⟩ slip, a high average SF of 0.417 is achieved along 45° direction in TBE sheets because of TD-deflected texture, resulting in the improved plasticity and bendability.

Acknowledgments

The authors are grateful for the financial supports from the National Natural Science

Foundation of China (Nos. U1764253, 51971044, U1910213, 52001037, U2037601), the Qinghai Scientific & Technological Program, China (No. 2018-GX-A1) and the Natural Science Foundation of Chongqing, China (No. cstc2019jcyj-msxmX0234).

References

[1] POLLOCK T M. Weight loss with magnesium alloys [J]. Science, 2010, 328: 986−987.

[2] LIANG Xin-li, PENG Xiang, JI Hao, LIU Wen-cai, WU Guo-hua, DING Wen-jiang. Microstructure and mechanical properties of as-cast and solid solution treated Mg−8Li−*x*Al−*y*Zn alloys [J]. Transactions of Nonferrous Metals Society of China, 2021, 31: 925−938.

[3] WANG Qing-hang, JIANG Bin, CHEN Dao-lun, JIN Zhao-yang, ZHAO Ling-yu, YANG Qing-shan, HUANG Guang-sheng, PAN Fu-sheng. Strategies for enhancing the room-temperature stretch formability of magnesium alloy sheets: A review [J]. Journal of Materials Science, 2021, 56: 12965−12998.

[4] NIE J F, SHIN K S, ZENG Z R. Microstructure, deformation, and property of wrought magnesium alloys [J]. Metallurgical and Materials Transactions A, 2020, 51: 6045−6109.

[5] JIANG M G, XU C, YAN H, FAN G H, NAKATA T, LAO C S, CHEN R S, KAMADO S, HAN E H, LU B H. Unveiling the formation of basal texture variations based on twinning and dynamic recrystallization in AZ31 magnesium alloy during extrusion [J]. Acta Materialia, 2018, 157: 53−71.

[6] GU Guang-lin, KE Xiang-nan, HU Fa-ping, ZHAO Shu-jie, WEI Guo-bin, YANG Yan, PENG Xiao-dong, XIE Wei-dong. Fine-grained Mg–1Mn–0.5Al–0.5Ca–0.5Zn alloy with high strength and good ductility fabricated by conventional extrusion [J]. Transactions of Nonferrous Metals Society of China, 2022, 32: 483−492.

[7] CHANG Li-li, GUO Jing, SU Xiao-jing. Effect of Y on microstructure evolution and mechanical properties of Mg−4Li−3Al alloys [J]. Transactions of Nonferrous Metals Society of China, 2021, 31: 3691−3702.

[8] WANG Ye, LI Feng, BIAN Nan, DU Hua-qiu, DA Huo-peng. Mechanism of plasticity enhancement of AZ31B magnesium alloy sheet by accumulative alternating back extrusion [J]. Journal of Magnesium and Alloys, 2023, 11: 1791−1801.

[9] LIANG Min-jie, ZHENG Jie, LIU Huan, YAO Bao-xing. Microstructure and mechanical properties of AZ31 alloy prepared by cyclic expansion extrusion with asymmetrical extrusion cavity [J]. Transactions of Nonferrous Metals Society of China, 2022, 32: 122−133.

[10] KIM W J, HONG S I, KIM Y S, MIN S H, JEONG H T, LEE J D. Texture development and its effect on mechanical properties of an AZ61 Mg alloy fabricated by equal channel angular pressing [J]. Acta Materialia, 2003, 51: 3293−3307.

[11] KASAEIAN N M, SEDIGHI M, HASHEMI R. Severe plastic deformation (SPD) of biodegradable magnesium alloys and composites: A review of developments and prospects [J]. Journal of Magnesium and Alloys, 2022, 10: 938−955.

[12] AHMADI S, ALIMIRZALOO V, FARAJI G, DONIAVI A. Properties inhomogeneity of AM60 magnesium alloy processed by cyclic extrusion compression angular pressing followed by extrusion [J]. Transactions of Nonferrous Metals Society of China, 2021, 31: 655−665.

[13] ORLOV D, RAAB G, LAMARK T T, POPOV M, ESTRIN Y. Improvement of mechanical properties of magnesium alloy ZK60 by integrated extrusion and equal channel angular pressing [J]. Acta Materialia, 2011, 59: 375−385.

[14] CHEN Liang, CHENG Qian, TANG Jian-wei, LI Zhi-gang, ZHAO Guo-qun, ZUO Yang. Numerical and experimental study on extrusion of ZK60 Mg alloy using billet with temperature gradient [J]. Journal of Materials Research and Technology, 2021, 14: 3018−3028.

[15] CHANG L L, WANG Y N, ZHAO X, HUANG J C. Microstructure and mechanical properties in an AZ31 magnesium alloy sheet fabricated by asymmetric hot extrusion [J]. Materials Science and Engineering A, 2008, 496: 512−516.

[16] XU Jun, YANG Tian-hao, JIANG Bin, SONG Jiang-feng, HE Jun-jie, WANG Qing-hang, CHAI Yan-fu, HUANG Guang-sheng, PAN Fu-sheng. Improved mechanical properties of Mg−3Al−1Zn alloy sheets by optimizing the extrusion die angles: Microstructural and texture evolution [J]. Journal of Alloys and Compounds, 2018, 762: 719−729.

[17] YANG Qing-shan, JIANG Bin, ZHOU Guan-yu, DAI Jia-hong, PAN Fu-sheng. Influence of an asymmetric shear deformation on microstructure evolution and mechanical behavior of AZ31 magnesium alloy sheet [J]. Materials Science and Engineering A, 2014, 590: 440−447.

[18] WANG Qing-hang, SONG Jiang-feng, JIANG Bin, TANG Ai-tao, CHAI Yan-fu, YANG Tian-hao, HUANG Guang-sheng, PAN Fu-sheng. An investigation on microstructure, texture and formability of AZ31 sheet processed by asymmetric porthole die extrusion [J]. Materials Science and Engineering A, 2018, 720: 85−97.

[19] GAO C Y, ZHANG L C, GUO W G, LI Y L, LU W R, KE Y L. Dynamic plasticity of AZ31 magnesium alloy: Experimental investigation and constitutive modeling [J]. Materials Science and Engineering A, 2014, 613: 379−389.

[20] RAKSHITH M, SEENUVASAPERUMAL P. Review on the effect of different processing techniques on the microstructure and mechanical behaviour of AZ31 Magnesium alloy [J]. Journal of Magnesium and Alloys, 2021, 9: 1692−1714.

[21] HU H J. A three-dimensional finite element simulation of the warm extrusion of AZ31 alloy billets [J]. Journal of Manufacturing Processes, 2010, 12: 67−72.

[22] LASER T, NÜRNBERG M R, JANZ A, HARTIG C, LETZIG D, SCHMID-FETZER R, BORMANN R. The influence of manganese on the microstructure and mechanical properties of AZ31 gravity die cast alloys [J]. Acta Materialia, 2006, 54: 3033−3041.

[23] ZENG Z R, ZHU Y M, LIU R L, XU S W, DAVIES C H J, NIE J F, BIRBILIS N. Achieving exceptionally high strength in Mg3Al1Zn−0.3Mn extrusions via suppressing intergranular deformation [J]. Acta Materialia, 2018, 160:

97−108.

[24] HUANG Xin-sheng, SUZUKI K, WATAZU A, SHIGEMATSU I, SAITO N. Improvement of formability of Mg−Al−Zn alloy sheet at low temperatures using differential speed rolling [J]. Journal of Alloys and Compounds, 2009, 470: 263−268.

[25] YANG Qing-shan, JIANG Bin, TIAN Yuan, LIU Wen-jun, PAN Fu-sheng. A tilted weak texture processed by an asymmetric extrusion for magnesium alloy sheets [J]. Materials Letters, 2013, 100: 29−31.

[26] YANG Q S, JIANG B, ZHOU G Y, HE J J, PAN F S. Enhancing strength and ductility of AZ31 magnesium alloy sheets by the trapezoid extrusion [J]. Materials Science and Technology, 2013, 30: 227−230.

[27] CHEN Yong-jun, WANG Qu-dong, PENG Jian-guo, ZHAI Chun-qun, DING Wen-jiang. Effects of extrusion ratio on the microstructure and mechanical properties of AZ31 Mg alloy [J]. Journal of Materials Processing Technology, 2007, 182: 281−285.

[28] JIN Zhong-zheng, CHENG Xiu-ming, ZHA Min, RONG Jian, ZHANG Hang, WANG Jin-guo, WANG Cheng, LI Zhi-gang, WANG Hui-yuan. Effects of Mg17Al12 second phase particles on twinning-induced recrystallization behavior in Mg−Al−Zn alloys during gradient hot rolling [J]. Journal of Materials Science & Technology, 2019, 35: 2017−2026.

[29] LI Jing-ren, ZHANG Ai-yue, PAN Hu-cheng, REN Yu-ping, ZENG Zhuo-ran, HUANG Qin-yan, YANG Chang-lin, MA Li-feng, QIN Gao-wu. Effect of extrusion speed on microstructure and mechanical properties of the Mg−Ca binary alloy [J]. Journal of Magnesium and Alloys, 2021, 9: 1297−1303.

[30] LIU X Q, QIAO X G, PEI R S, CHI Y Q, YUAN L, ZHENG M Y. Role of extrusion rate on the microstructure and tensile properties evolution of ultrahigh-strength low-alloy Mg−1.0Al−1.0Ca−0.4Mn (wt.%) alloy [J]. Journal of Magnesium and Alloys, 2023, 11: 553−561.

[31] BAI Sheng-wen, FANG Gang, ZHOU Jie. Investigation into the extrudability of a new Mg−Al−Zn−RE alloy with large amounts of alloying elements [J]. Metallurgical and Materials Transactions A, 2019, 50: 3246−3264.

[32] WANG Li-fei, LI Yong-qiao, ZHANG Hua, ZHANG Zheng-yong, YANG Qingshan, ZHANG Qiang, WANG Hong-xia, CHENG Wei-li, SHIN K S, VEDANI M. Review: Achieving enhanced plasticity of magnesium alloys below recrystallization temperature through various texture control methods [J]. Journal of Materials Research and Technology, 2020, 9: 12604−12625.

[33] CHEN Shuai-feng, SONG Hong-wu, CHENG Ming, ZHENG Ce, ZHANG Shi-hong, LEE M G. Texture modification and mechanical properties of AZ31 magnesium alloy sheet subjected to equal channel angular bending [J]. Journal of Materials Science & Technology, 2021, 67: 211−225.

[34] SONG Bo, YANG Qing-shan, ZHOU Tao, CHAI Lin-jiang, GUO Ning, LIU Ting-ting, GUO Sheng-feng, XIN Ren-long. Texture control by $\{10\bar{1}2\}$ twinning to improve the formability of Mg alloys: A review [J]. Journal of Materials Science & Technology, 2019, 35: 2269−2282.

[35] AGNEW S R, YOO M H, TOMÉ C N. Application of texture simulation to understanding mechanical behavior of Mg and solid solution alloys containing Li or Y [J]. Acta Materialia, 2001, 49: 4277−4289.

[36] LYU Shao-yuan, XIAO Wen-long, LI Guo-dong, XIA Da-biao, HUANG Yuan-ding, GAVRAS S, HORT N, ZHENG Rui-xiao, MA Chao-li. Formation mechanism of the abnormal texture during extrusion in Mg−Y−Sm−Zn−Zr alloy [J]. Journal of Alloys and Compounds, 2020, 821: 153477.

[37] BARNETT M R. A taylor model based description of the proof stress of magnesium AZ31 during hot working [J]. Metallurgical and Materials Transactions A, 2003, 34: 1799−1806.

[38] WANG Qing-hang, JIANG Bin, TANG Ai-tao, HE Chao, ZHANG Ding-fei, SONG Jiang-feng, YANG Tian-hao, HUANG Guang-sheng, PAN Fu-sheng. Formation of the elliptical texture and its effect on the mechanical properties and stretch formability of dilute Mg−Sn−Y sheet by Zn addition [J]. Materials Science and Engineering A, 2019, 746: 259−275.

[39] AGIUS D, KAREER A, MAMUN A A, TRUMAN C, COLLINS D M, MOSTAFAVI M, KNOWLES D. A crystal plasticity model that accounts for grain size effects and slip system interactions on the deformation of austenitic stainless steels [J]. International Journal of Plasticity, 2022, 152: 103249.

[40] KUANG Jie, ZHANG Yu-qing, DU Xin-peng, ZHANG Jin-yu, LIU Gang, SUN Jun. On the strengthening and slip activity of Mg−3Al−1Zn alloy with pre-induced $\{10\bar{1}2\}$ twins [J]. Journal of Magnesium and Alloys, 2021, 11: 1292−1307.

[41] JEONG J, ALFREIDER M, KONETSCHNIK R, KIENER D, OH S H. In-situ TEM observation of $\{10\bar{1}2\}$ twin-dominated deformation of Mg pillars: Twinning mechanism, size effects and rate dependency [J]. Acta Materialia, 2018, 158: 407−421.

[42] WANG Qing-hang, CHEN Si-yuan, JIANG Bin, JIN Zhaoyang, ZHAO Ling-yu, HE Jun-jie, ZHANG Ding-fei, HUANG Guang-sheng, PAN Fu-sheng. Grain size dependence of annealing strengthening of an extruded Mg−Gd−Zn alloy subjected to pre-compression deformation [J]. Journal of Magnesium and Alloys, 2022, 10: 3576−3588.

[43] WANG Hui-yuan, FENG Ting-ting, ZHANG Lei, LIU Chun-guo, PAN Yue, ZHA Min, NAN Xiao-long, WANG Cheng, JIANG Qi-chuan. Achieving a weak basal texture in a Mg−6Al−3Sn alloy by wave-shaped die rolling [J]. Materials & Design, 2015, 88: 157−161.

[44] PARK S H, HONG S G, LEE J H, HUH Y H. Texture evolution of rolled Mg−3Al−1Zn alloy undergoing a $\{10\bar{1}2\}$ twinning dominant strain path change [J]. Journal of Alloys and Compounds, 2015, 646: 573−579.

[45] YANG W, QUAN G F, JI B, WAN Y F, ZHOU H, ZHENG J, YIN D D. Effect of Y content and equal channel angular pressing on the microstructure, texture and mechanical property of extruded Mg−Y alloys [J]. Journal of Magnesium and Alloys, 2022, 10: 195−208.

[46] HE Jun-jie, MAO Yong, GAO Yu-ping, XIONG Kai, JIANG Bin, PAN Fu-sheng. Effect of rolling paths and pass

reductions on the microstructure and texture evolutions of AZ31 sheet with an initial asymmetrical texture distribution [J]. Journal of Alloys and Compounds, 2019, 786: 394−408.

[47] SONG Deng-hui, ZHOU Tao, TU Jian, SHI Lai-xin, SONG Bo, HU Li, YANG Ming-bo, CHEN Qiang, LU Li-wei. Improved stretch formability of AZ31 sheet via texture control by introducing a continuous bending channel into equal channel angular rolling [J]. Journal of Materials Processing Technology, 2018, 259: 380−386.

[48] XU Jun, JIANG Bin, KANG Yue-hua, ZHAO Jun, ZHANG Wei-wen, ZHENG Kai-hong, PAN Fu-sheng. Tailoring microstructure and texture of Mg−3Al−1Zn alloy sheets through curve extrusion process for achieving low planar anisotropy [J]. Journal of Materials Science & Technology, 2022, 113: 48−60.

[49] LI Fei-Fan, FANG Gang. Modeling of 3D plastic anisotropy and asymmetry of extruded magnesium alloy and its applications in three-point bending [J]. International Journal of Plasticity, 2020: 130: 102704.

[50] HE Chao, JIANG Bin, WANG Qing-hang, CHAI Yan-fu, ZHAO Jun, YUAN Ming, HUANG Guang-sheng, ZHANG Ding-fei, PAN Fu-sheng. Effect of precompression and subsequent annealing on the texture evolution and bendability of Mg−Gd binary alloy [J]. Materials Science and Engineering A, 2021: 799: 140290.

[51] SINGH J, KIM M S, CHOI S H. The effect of initial texture on micromechanical deformation behaviors in Mg alloys under a mini-V-bending test [J]. International Journal of Plasticity, 2019, 117: 33−57.

[52] HE Chao, YUAN Ming, JIANG Bin, LIU Lin-tao, WANG Qing-hang, CHAI Yan-fu, LIU Wen-jun, HUANG Guang-sheng, ZHANG Ding-fei, PAN Fu-sheng. Anomalous effect of grain size on the room-temperature bendability of Mg−Gd alloy sheet [J]. Materials Science and Engineering A, 2022: 832: 142397.

[53] KNEZEVIC M, LEVINSON A, HARRIS R, MISHRA R K, DOHERTY R D, KALIDINDI S R. Deformation twinning in AZ31: Influence on strain hardening and texture evolution [J]. Acta Materialia, 2010, 58: 6230−6242.

[54] CHAPUIS A, LIU Pei, LIU Qing. An experimental and numerical study of texture change and twinning-induced hardening during tensile deformation of an AZ31 magnesium alloy rolled plate [J]. Materials Science and Engineering A, 2013, 561: 167−173.

基于弯曲定径带模具挤压的 Mg−3Al−1Zn 合金力学性能优化

刘林涛[1]，白生文[1]，蒋 斌[1,2]，何 超[1]，王庆航[3]，袁 明[1]，黄光胜[1]，张丁非[1]，潘复生[1,2]

1. 重庆大学 国家镁合金材料工程技术研究中心，重庆 400044；
2. 重庆科学技术研究院，重庆 401123；
3. 扬州大学 机械工程学院，扬州 225127

摘 要：设计了一种采用弯曲定径带模具的新型非对称挤压工艺(TBE)，用以改善 Mg−3Al−1Zn 合金板材的力学性能和成形性能。运用有限元分析揭示了挤压过程中的应变、温度等状态变量的分布。结果表明，在 TBE 模具的模口处，应变沿板面法向(ND)呈梯度分布，这导致挤压板材显微组织的厚向梯度分布，同时得到 TD 择优取向的织构，少量基面取向晶粒向挤压方向(ED)偏转。与传统挤压相比，TBE 过程中产生更多挤压热，模腔内温度更高，使大量非基面滑移开启，导致板材 TD 择优取向织构的形成。通过改善织构，TBE 板材的塑性和弯曲性能均得到明显提升，沿 45°方向的伸长率达到 33%，弯曲角度达到 83.5°。

关键词：弯曲定径带挤压；TD 择优取向织构；塑性；弯曲性能；梯度晶粒尺寸

(Edited by Bing YANG)